CrossMark

ORIGINAL PAPER

Numerical Simulation of Possible Evolution Scenarios of the Rosone Deep-Seated Gravitational Slope Deformation (Italian Alps, Piedmont)

Marina Pirulli[1]

Abstract The large, deep-seated Rosone landslide (Western Italian Alps) has been known since the beginning of the twentieth century as an active phenomenon characterized by a slow but constant evolution. Its possible evolution, in terms of a catastrophic rock avalanche, could have serious consequences on several elements at risk, including a hydroelectric power plant. Runout estimates are needed to identify the potential impact on the territory of such an event and, when possible, to minimize hazard areas. This article analyses the evolution of three potential rock avalanche scenarios, with decreasing probability of occurrence and increasing impact on land planning. A comparison between runout results obtained by other authors and some new analyses that have been carried out with the three-dimensional continuum mechanics-based RASH^{3D} code is made and commented on by highlighting the advantages, but also the limits, of using a more complete tool, such as RASH^{3D}.

Keywords Deep-seated gravitational slope deformation · Rock avalanche · Numerical modeling · Continuum mechanics

1 Introduction

The increasing population density and the development of mountainous terrain make human settlements subjected to landslides. The most serious threat probably arises from small, high-frequency landslides, such as debris flows and debris avalanches. However, large and relatively rare rock avalanches also constitute a significant hazard, due to their prodigious capacity for destruction. Such landslides can involve the spontaneous failure of entire mountain slopes, with volumes of some tens or hundreds of millions m^3 and travel distances of several km (Hungr 2006).

The "rock avalanche" term has developed naturally in literature, as a simplification of the complicated "rock slide-debris avalanche" term, proposed by Varnes (1978). Hungr et al. (2001) suggested that the "rock avalanche" term should be reserved for flow-like movements of fragmented rock resulting from major, extremely rapid rock slides. This contrasts with the "debris avalanche" term, which should be used to describe landslides that originate in unconsolidated material. However, many rock avalanches entrain unconsolidated debris along their long travel paths. Hungr et al. (2001) recommended that the "rock slide-debris avalanche" term be used when a rock slide mobilizes a large quantity of debris through entrainment of a liquefied substrate from the path.

A stability analysis of entire mountain slopes is exceedingly difficult. As a consequence, interest in the possible occurrence of a rock avalanche usually arises only once certain precursory signs of impending failure appear. Once such signs have been identified, the monitoring of displacements, strains, piezometric pressures or rock noise can be used to gauge the deterioration in stability and to signal the onset of failure.

As already mentioned, the stabilization of potential rock avalanche sources is only possible in exceptional cases. Under normal circumstances, such stabilization projects are not economically feasible. Hazard mitigation can only be achieved by removing vulnerable structures from the path of the potential landslide. For this purpose, a reliable runout analysis is required.

✉ Marina Pirulli
marina.pirulli@polito.it

[1] Department of Structural, Geotechnical and Building Engineering, Politecnico di Torino, Corso Duca degli Abruzzi, 24, 10129 Turin, Italy

Since rock avalanches have rarely been observed directly, very little direct data relevant to their dynamics exist (Sosio et al. 2008) and modeling calibration usually relies on evidences such as the mudline records of superelevations in bends, debris extensions and elevations, runups, erosion depths, deposit thicknesses and branching.

The purpose of this article is to give a brief description of the Rosone deep-seated gravitational slope deformation and to describe its possible evolution, in terms of catastrophic rock avalanche, by evidencing the contribution that the application of a numerical code, based on a continuum mechanics approach, such as RASH^{3D} (Pirulli 2005), can give.

The potential evolution of this rock avalanche has already been investigated by Forlati et al. (Forlati et al. 1991) using a simple empirical approach based on the formulations of Scheidegger (1973) and Li (1983). A similar but more detailed analysis was carried out in 2001 by Enel.Hydro, using Friz and Pinelli's empirical approach (1993). Finally, in 2004, the application of the pseudo-three-dimensional DAN code (Hungr 1995) to one of the possible evolution scenarios of a Rosone rock avalanche (Pirulli 2004) allowed an improvement to be made in the knowledge of the mass behavior during the propagation and the deposition phases. The obtained results not only refer to the runout distance, but also to the landslide velocity, the time at which the event finishes and the depth of the displaced mass once it comes to a stop.

Unlike all the previous runout analyses, the RASH^{3D} code allows the possible evolution of the movement to be investigated on a real complex three-dimensional topography.

A detailed description of the RASH^{3D} results and a comparison with the results of previous analyses are given in the following sections.

2 Description of the Rosone Landslide

The so-called Rosone landslide is located in the Orco river valley (Italian Western Alps, Fig. 1) and it is classified as a deep-seated gravitational slope deformation (DSGSD). It has been known, since the beginning of the twentieth century, as an active phenomenon characterized by a slow yet constant evolution with periodical accelerations (e.g., Forlati et al. 1991; Luino et al. 1993; Ramasco and Troisi 2003; Amatruda et al. 2004). This DSGSD affects an area of about 5.5 km^2, which ranges from 700 to 2000 m asl and reaches great depths (Forlati et al. 2001).

On the basis of its morphological characteristics, Ramasco et al. (1989) divided the sliding mass into three main sectors according to the different evolutional stages: Ronchi, Perebella, Bertodasco (Fig. 2).
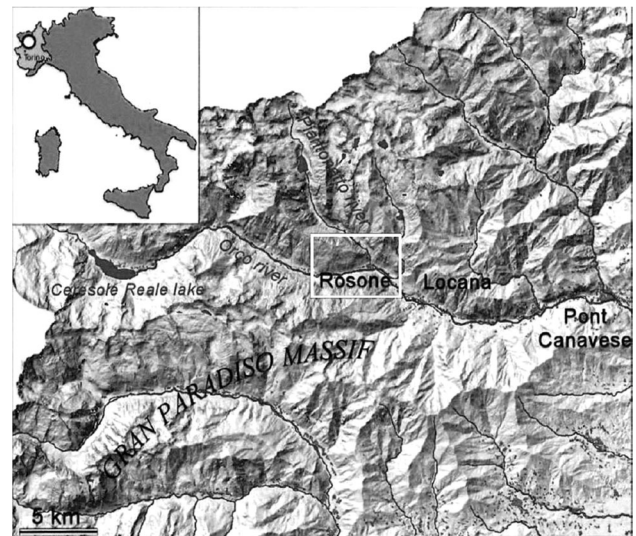
Fig. 1 Location of the Rosone landslide (modified after Pisani et al. 2010)

Since the Bertodasco sector has been identified as the most likely to undergo a catastrophic evolution, and two important inhabited zones are located around this sector: the village of Rosone and the hydro-power plant, presently owned by the City of Turin Electricity Board, IRIDE S.p.A. (Fig. 2), this sector is the most intensely investigated and well known sector.

Water, drawn from the Ceresole Reale dam, is sent to some pools through a 17-km-long gallery tank, and falls toward the power plant inside a penstock, which covers almost the entire length of the landslide, with a drop of 813 m (Fig. 2).

The landslide also involves the N 460 National Road from Turin to Ceresole Reale, which runs along the valley bottom.

2.1 Geological and Structural Settings

The Orco valley is located in the central part of the Gran Paradiso Massif (Pennine Domain), whose geological unit consists of a composite crystalline basement and a locally preserved Permo-Liassic cover (Compagnoni et al. 1974).

The Rosone landslide is modeled on the Augen Gneiss Complex. The geological–structural configuration of the studied area is relatively simple: granite and augen gneiss crop out (Delle Piane et al. 2010).

The deformation is controlled by structural settings and presents brittle behavior. Three main systems of discontinuities have been identified, namely: schistosity (SR in Fig. 3; dip direction 154°, dip 34°), which is defined by regional metamorphic foliation, and two main joint systems, K1 and K2, with dip/dip direction of 85/100 and 68/015, respectively (Forlati et al. 2001).
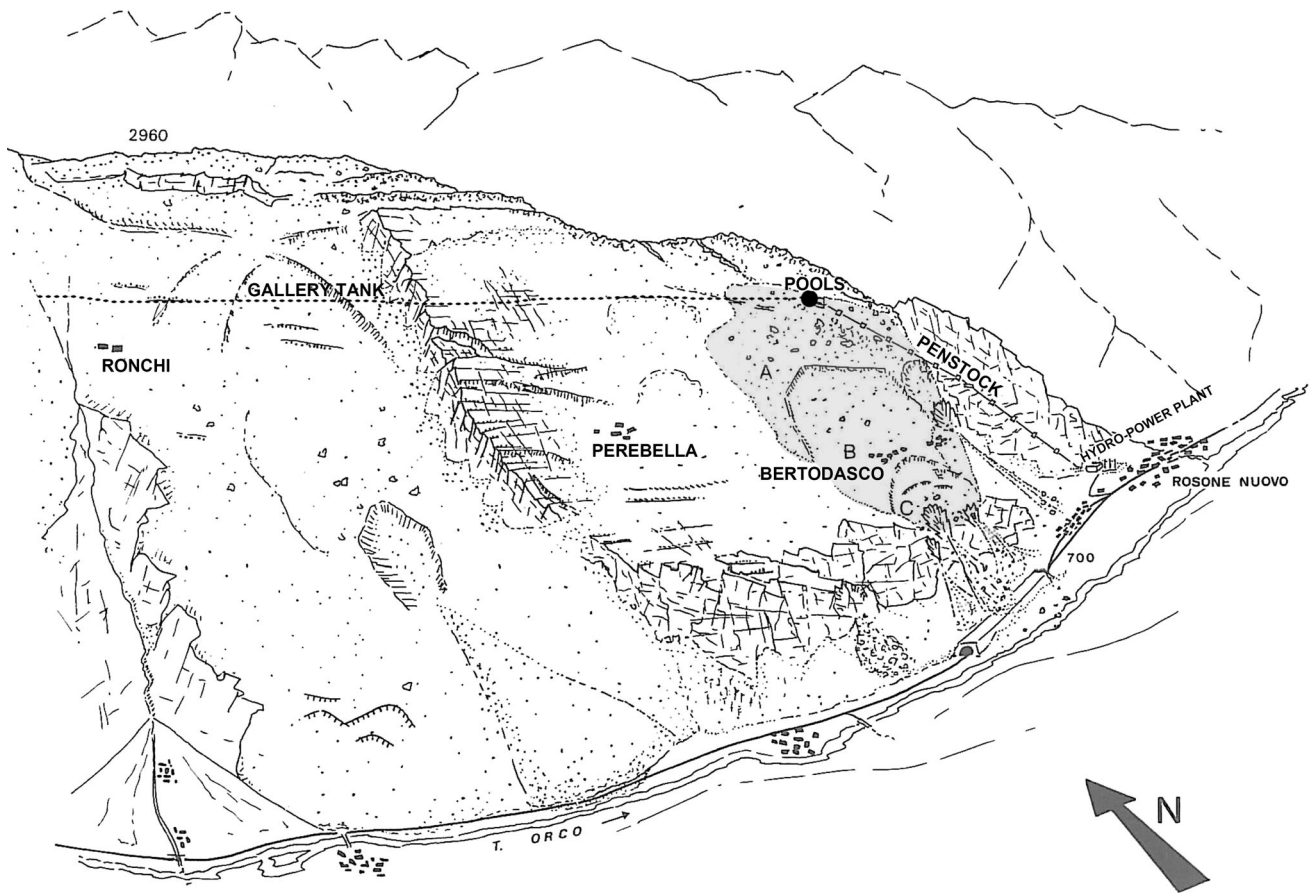
Fig. 2 Sketch of the Rosone deep-seated gravitational slope deformation (DSGSD) process (modified after Forlati et al. 1991) with indication of the three sectors: Ronchi, Perebella and Bertodasco. Each sector represents a different phase of the whole evolutionary process of the slope. As far as the Bertodasco sector is concerned, the *A*, *B* and *C letters* are used to identify the three different types of movements that characterize this sector, and whose details are given in § 2.2
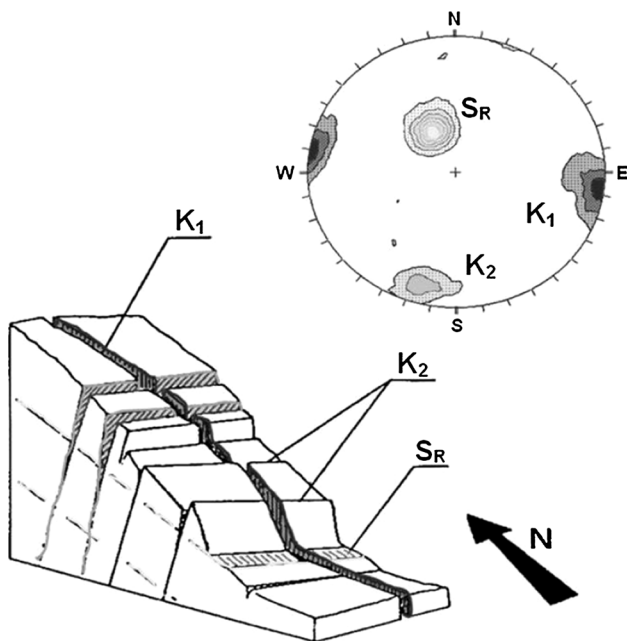
Fig. 3 3D sketch of the main tectonic discontinuities of the Rosone area (modified after Forlati et al. 2001)

The two main orthogonal fracture systems (K1 and K2) in the Perebella sector display wide open fractures and, in some cases, simply juxtaposed rock elements. However, the three discontinuity systems are also locally evident in the Bertodasco sector, even though it is much more chaotic and disrupted (Pisani et al. 2010).

The upper part of the Bertodasco sector has several trenches perpendicular to the main direction of the slope movement, whereas the middle part is affected by rotational sliding movements as well as general toppling and planar slides.

2.2 Field Estimation of the Sliding Volumes

On the basis of the morphological and structural characteristics, inclinometric measurements, surface deformation measurements, seismic imaging and laboratory tests that have been carried out since 1929, the Bertodasco sector, has already mentioned, has been identified as the most active part of the DSGSD (Fig. 4).

Fig. 4 Geomorphological map of the Rosone area with an example of monitoring data results based on persistent scattered data (modified after Notti et al. 2013a, b)
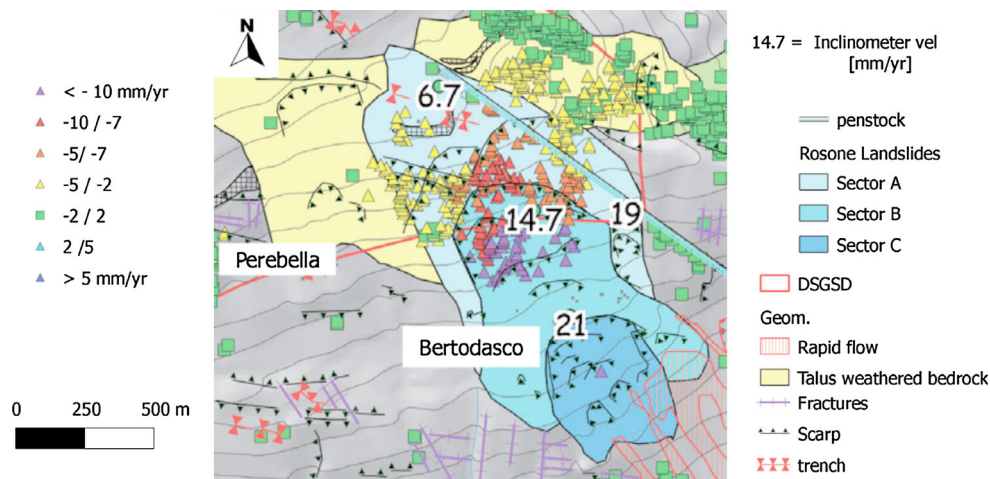
Fig. 5 Bertodasco sector with delimitation of its three main areas according to Forlati et al. (1991)
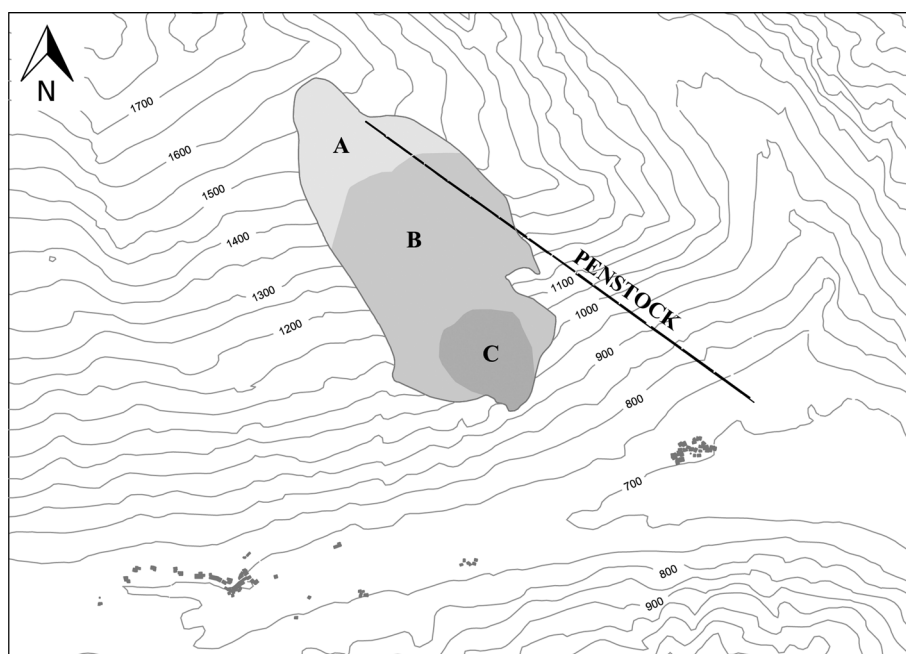
For this reason, attention has been focused on this sector, and in particular, considering the above-mentioned investigations, Forlati et al. 1991 subdivided it into three main sectors with different rock mass evolutions and movements, referred to as A, B and C, going from the top to the bottom of the valley (Fig. 5).

As a consequence, the following three different evolution scenarios, with decreasing probability of occurrence and increasing impact on land planning, have been taken into account:

Scenario 1 Zone C (Fig. 5). The rock mass in Zone C is heavily fractured and disarticulated. The sliding surface is about 40/60 m deep. The type of movement is mainly roto-translational. This sector is also affected by rock falls and debris flows. In 1953, a reactivation of the movement caused severe damage to the Bertodasco village, and the inhabitants were evacuated. The volume of the entire slide can be estimated as about 2.4×10^6 m^3.

Scenario 2 Zones B and C (Fig. 5). The collapse of Zone C could cause the collapse of Zone B at the same time. The rock mass in sector B is rather weathered, with completely disarticulated rock blocks, scarps and the presence of a great deal of debris. The sliding surface has been identified at a depth of 40/50 m, and the type of movement is mainly planar. The total volume involved in this scenario would be of about 11.7×10^6 m^3.

Scenario 3 Zones A, B and C (Fig. 5). The collapse of Zones C and B could induce the failure of the whole rock body that would involve a volume of about 22.7×10^6 m³. The rock mass in Zone A presents very few deformations and it is quite compact. However, many trenches and scarps can be detected. The sliding surface is between 30 and 75 m deep and the movement is generally weak. Because of the small recorded displacements, this scenario should be considered less probable than the previous ones.

2.3 Occurrence Probability

The estimation of the probability of sliding is one of the critical components of the assessment of landslide risks and hazards for natural and constructed slopes. The probability of sliding can be estimated using probabilistic analysis approaches (e.g., Fell et al. 2007) which are inherently quantitative in nature, or using semi-quantitative methods based on historical records, geomorphology, rainfall, slope geometry, performance and other indications.

In the case of the Rosone landslide, quantitative methods could not be applied because the uncertainty in the definition of the parameters involved is too large and it was not possible to define any reliable variability for these parameters (Amatruda et al. 2004).

Since several historical records on the landslide activity in the area existed, Amatruda et al. (2004) applied the historical approach to the Rosone case: in this way, it was possible to obtain information related to the periodic frequency of events.

An occurrence time range was obtained, from the historical data analysis, for each scenario, considering the minimum and maximum time intervals between two consecutive recorded events. On the basis of their mean values, the frequency indicated in Table 1 was calculated, in terms of events per year (Amatruda et al. 2004).

3 Description of the Different Methodologies Used to Analyze a Potential Rock Avalanche Event

The consequence of the possible evolution of the Rosone rock avalanche has been studied by different authors and using different methodologies.

A description of the different approaches is given in the following sub-sections.

3.1 Scheidegger's (1973) and Li's (1983) Empirical Methodologies

Empirical methods can roughly predict the overall travel distance of a landslide mass, or its areal extent, but they give no indication of the distribution of debris in the deposition area, information that is needed for the planning of protective measures (Hungr 2002).

Heim (1932), on the basis of empirical observations, ascertained the dependence of the distance traveled by the rock mass (L) upon the initial height (H), the regularity of the terrain and the volume of the landslide (V). He defined the slope (α) of a line drawn between the crown of the source area and the toe of the deposit, measured on a straightened profile of the path, as "Fahrböschung".

Since first introduced by Heim, correlations between the angle of reach and changes in the landslide volume, type and runout path have been investigated by many authors. For example, Forlati et al. 1991 used the Scheidegger (1973) and Li (1983) methods to analyze a potential Rosone landslide.

Scheidegger (1973) formalized Heim's relationship by defining a correlation between landslide volume (V) and the ratio of the total fall height (H) to the total runout distance (L). Considering data from 33 prehistoric and historic rock avalanches, regression Eq. 1 was obtained.

$$\log\left(\frac{H}{L}\right) = -0.15666 \cdot \log V + 0.62419 \tag{1}$$

Li (1983) examined a sample of 76 landslides to find a correlation between volume and H/L, as well as between the landslide volume and the spreading area. Disregarding all events with volumes of less than 10^5 m³, he obtained an equation for the regression of landslide propagation (L) which is similar to that obtained by Scheidegger, namely,

$$\log\left(\frac{H}{L}\right) = -0.1529 \cdot \log V + 0.6640 \tag{2}$$

and an indication of the area (A) affected by the arrival of landslide debris, that is:

Table 1 Frequency of each scenario calculated in terms of events per year (modified after Amatruda et al. 2004)

Scenario	Occurrence range (years)	Average (years)	Frequency (event/year)
1	0 ÷ 50	25	1/25 = 0.04
2	50 ÷ 250	150	1/150 = 0.007
3	>250	1000	1/1000 = 0.001

$$\log A = 1.9 + 0.57 \cdot \log V \tag{3}$$

3.2 Friz and Pinelli's Empirical Methodology (1993)

The three previously described scenarios were analyzed in 2001 by Enel.Hydro using the Friz and Pinelli's empirical methodology (1993), which is based on both mechanical and statistical considerations (Perla et al. 1980; Li 1983; Dutto and Friz 1989). The simple two-parameter model of Perla et al. (1980) was applied to define both the maximum axial sliding distance (R_a, Fig. 6b) and the maximum lateral sliding distance (R_l, Fig. 6c). The unstable mass was considered as a dimensionless block that slides on an assigned topography, and which is subjected to gravity and
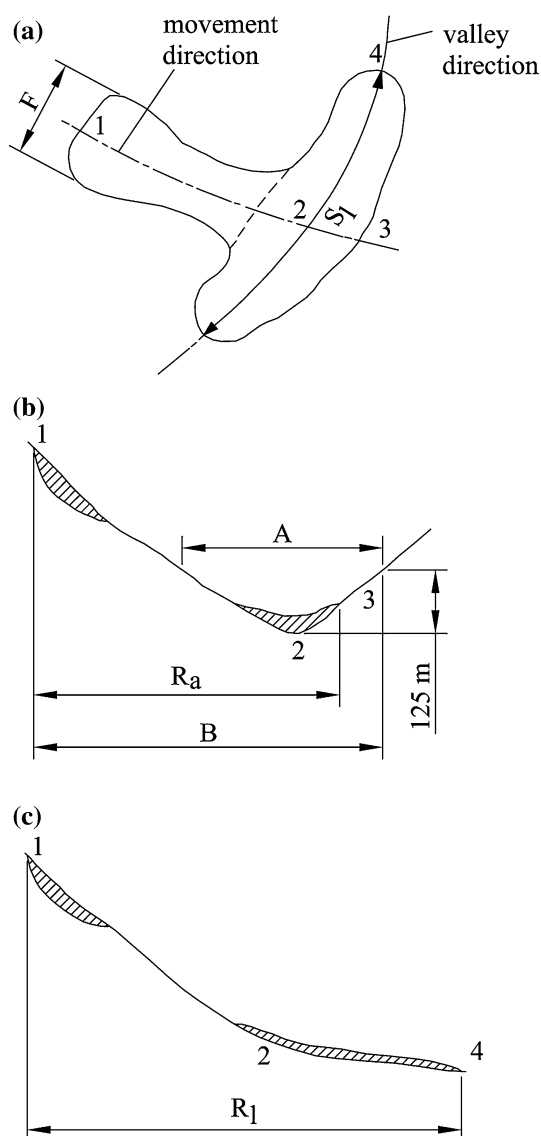
Fig. 6 Definition of the geometrical parameters used in Friz and Pinelli's methodology (1993)

basal resisting forces. The dynamic friction coefficient (μ) is obtained using the following.

$$\mu = 0.173 + 0.0024 K_f - 0.0007V \tag{4}$$

where V is the volume of the event in millions of cubic meters and K_f is a shape coefficient which considers the transversal section of the valley in the direction of propagation of the flowing mass. Moreover,

$$K_f = \left(1 - \frac{A}{B}\right) \cdot 100 \tag{5}$$

where A is the width of the valley, conventionally measured in the direction of the mass propagation at 125 m above the valley bottom, and B is the horizontal distance from the upper limit of the potentially unstable volume and the horizontal projection of the distal point of the A segment on the opposite slope (Fig. 6b).

As far as the R_l determination is concerned, it should be pointed out that the estimation of this aspect hypothesized that once the mass reaches the bottom of the valley, its propagation direction changes and it immediately starts to follow the direction of the valley bottom (Fig. 6c).

The maximum lateral expansion (S_l, Fig. 6a) was instead obtained from a multiple regression analysis, made considering the lateral expansion (S_l), the front width (F) and the volume (V) of a large number of historical cases (Friz and Pinelli 1993). The following relation was obtained:

$$S_l = -235.9 + 2.43F + 1.99V \tag{6}$$

where F is the width of the flow front at triggering (Fig. 6a) and V is the volume of the event in millions of cubic meters.

Since R_a and S_l are point parameters, the shape of the possible runout area was obtained by Enel.Hydro through graphical interpretation of the topography. The runout area was not assumed as symmetrical to the axial travel distance, but was shifted taking into account a prevalent expansion of the mass in the direction of the valley (see the solid black line in Figs. 10, 11 and 12).

3.3 The Numerical Modeling Based on a Continuum Mechanics Approach: from DAN (Hungr 1995) to RASH^{3D} (Pirulli 2005)

The theoretical basis of both DAN and RASH^{3D} is a system of depth-averaged governing equations derived from continuum mechanics principles. The pseudo-three-dimensional DAN code, adopted by Pirulli (2004) to study Scenario 1 of the Rosone potential landslide, uses a one-dimensional form of the equations of motion, while the three-dimensional RASH^{3D} code, whose application to all the possible Rosone evolution scenarios is presented in this paper, uses a two-dimensional form of the same equations.

The assumption of a homogeneous continuum material (e.g., Savage and Hutter 1989; Iverson and Denlinger 2001) is supported by the observation that the depth and length of a flowing mass are usually larger than the characteristic dimensions of the single particles involved in the movement. It, therefore, becomes possible to find an "equivalent" fluid within these limits whose rheological properties are such that the bulk behavior of the flowing body can simulate the expected bulk behavior of the real landslide.

It follows that the evolution of the avalanche mass is governed by mass and momentum conservation laws, namely

$$\nabla \cdot v = 0 \tag{7}$$

$$\rho\left(\frac{\partial v}{\partial t} + v \cdot \nabla v\right) = -\nabla \cdot \sigma + \rho g \tag{8}$$

in which $v = (v_x, v_y, v_z)$ denotes the three-dimensional velocity vector of the avalanche in a (x, y, z) coordinate system, σ is the Cauchy stress tensor, ρ the mass density and g the gravitational acceleration vector.

Assuming that the vertical structure of the flow is much smaller than the characteristic length, the balance equations can be integrated in depth, thus obtaining the so-called depth-averaged St. Venant equations (Savage and Hutter 1989). This depth-averaged approach, together with the assumption that most of the collisions and deformations are concentrated in the boundary layer near the bed surface (Kilburn and Sorensen 1998), allows changes in the mechanical behavior inside the flow to be ignored. The complex rheology of the moving material is, therefore, incorporated in a single term which describes the frictional stress that develops at the interface between the flowing material and the rough surface. Neglecting transverse shear stress, the equations that have to be solved are, therefore:

$$\begin{cases} \dfrac{\partial h}{\partial t} + \dfrac{\partial(\overline{v_x}h)}{\partial x} + \dfrac{\partial(\overline{v_y}h)}{\partial y} = 0 \\[2mm] \rho\left(\dfrac{\partial(\overline{v_x}h)}{\partial t} + \dfrac{\partial\left(\overline{v_x^2}h\right)}{\partial x} + \dfrac{\partial(\overline{v_x v_y}h)}{\partial y}\right) = -\dfrac{\partial(\overline{\sigma_{xx}}h)}{\partial x} + \tau_{zx} - \rho g_x h \\[2mm] \rho\left(\dfrac{\partial(\overline{v_y}h)}{\partial t} + \dfrac{\partial(\overline{v_y v_x}h)}{\partial x} + \dfrac{\partial\left(\overline{v_y^2}h\right)}{\partial y}\right) = -\dfrac{\partial(\overline{\sigma_{yy}}h)}{\partial y} + \tau_{zy} - \rho g_y h \end{cases} \tag{9}$$

where $\overline{v_x}, \overline{v_y}$ denote the depth-averaged flow velocity in the x and y directions, h the fluid depth, τ_{zx}, τ_{zy} are the shear stresses in the x and y directions, $\overline{\sigma_{xx}}, \overline{\sigma_{yy}}$ denote the depth-averaged stress in the x and y directions and g_x, g_y are the projections of the gravity vector along the x and y directions.

Equation 9 is solved in RASH[3D] using an Eulerian framework and a finite volume approach, which solves hyperbolic systems using the concept of cell-centered conservative quantities, developed by Audusse et al. (2000) and Bristeau and Coussin (2001) to compute Saint-Venant equations for hydraulic problems.

The one-dimensional form of Eq. 9 is instead solved in DAN with a Lagrangian framework as an extension of lumped mass models (e.g., Körner 1976; Hutchinson 1986).

Both codes allow a variety of material rheologies to be considered. It was then possible to simulate the dynamics of the Rosone event with a Frictional rheology in DAN (Pirulli 2004) and with both Frictional and Voellmy rheologies in RASH[3D].

The Frictional rheology is based on a constant friction angle φ, which implies a constant ratio of the shear stress to the normal stress. The shear resistance stresses, τ_{zi}, are independent of velocity:

$$\tau_{zi} = -(\rho g_z h \tan\varphi) \cdot \frac{\bar{v}_i}{\bar{v}} \tag{10}$$

where h is the flow depth, ρ is the material bulk density, g is the acceleration due to gravity and $\bar{v}$ the depth-averaged flow velocity.

The Voellmy rheology combines a Coulomb-based frictional term and a velocity-dependent turbulence parameter to account for velocity-dependent energy losses. The resulting basal shear stress, τ_{zi}, is given by the following equation:

$$\tau_{zi} = -\left(\rangle g_z h \mu + \frac{\rangle g \bar{v}_i^2}{\xi}\right) \cdot \frac{\bar{v}_i}{\bar{v}} \tag{11}$$

where ξ is the turbulence coefficient and μ is the friction coefficient. Voellmy (1955) developed this model empirically for snow avalanches by combining Coulomb's frictional formula and Chezy's formulas. The turbulence term, ξ, which is similar, although not exactly equivalent, to the Manning "n" term, was used to cover all the velocity-dependent factors in snow avalanche motion, including turbulence of the air–snow dispersion and air drag on the top surface of the avalanche (Hungr and Evans 2004). Körner (1976) showed that the model offers a good simulation of rock avalanche velocities, and it has been successfully applied to debris flows and debris avalanches by many authors (e.g., Rickenmann and Koch 1997; Revellino et al. 2004; Pirulli and Marco 2010).

4 Calibration of the RASH[3D] Numerical Analyses

To run RASH[3D] analyses, the following three steps have to be performed (1) uploading the topography of the study area as a digital elevation model (DEM), (2) defining the

triggering volume, and (3) selecting the rheology and setting its parameters.

Once a rheological relationship is chosen, the setting of its rheological parameter values, to define the flow characteristics, still remains an open question. As a consequence, the here discussed numerical results were obtained investigating a set of rheological values for each scenario and for each selected rheology. The range of variation of each rheological parameter was defined on the basis of a calibration-based approach.

In a calibration-based approach, the rheological parameters are constrained by means of systematic adjustment during the trial-and-error back-analysis of full-scale events. In this frame, the simulation of a historical event is usually achieved by matching the simulated travel distance, the velocities and the extent and depth of the deposit to those observed on site. The back-calculation of rheological parameters contributes to the understanding of the dynamics of past complex phenomena and can provide calibrated input parameters that can be used for first-order runout forward-analyses.

Taking into account that the effectiveness of the use of back-analyzed values in forward-analyses is a function of the degree of similarity between the characteristics of the back-analyzed cases and the potential event (e.g., Hungr and Evans 1996; Pirulli 2005; McDougall et al. 2008; Pirulli and Mangeney 2008), the dataset of the back-analyzed cases has to be subdivided on the basis of the type of phenomenon (e.g., rock avalanche, debris flow, etc.), event volume, path morphology, source and path material type and many other factors, thus introducing further constraints to the calibration results.

As an example, considering the path morphology, the potential Rosone rock avalanche can be compared to phenomena such as those of the Val Pola rock avalanche (Fig. 7a), which occurred in Italy in 1987 and involved a volume of about 30×10^6 m^3, and the Hope rock avalanche (Fig. 7b), which occurred in Canada in 1965 and involved an estimated volume of 47×10^6 m^3.

Considering the above-mentioned subdivision criteria, the first splitting criterion, suggested by Nicoletti and Sorriso-Valvo in 1991, was the subdivision of the rock avalanche dataset into three groups as a function of the path morphology (Fig. 8): elongated, tongue and T-shaped runout areas. All the above-mentioned examples of rock avalanche fall into the T-shaped runout areas.

As a result, the ranges of values given in Table 2 have been investigated with RASH^{3D} for the three Rosone landslide scenarios.

In the following section, the results obtained with RASH^{3D} are discussed and compared with the results obtained by other authors.

5 Results of RASH^{3D} Numerical Simulations and Comparison with Previous Results

Even though (1) the runout analyses carried out by Forlati et al. 1991 did not produce spatial distribution maps of the mass in the area affected by the propagation of the potential rock avalanche and (2) the results presented by Pirulli (2004) only concern one of the previously described scenarios (Scenario 1) and the runout area defined by Enel.Hydro (2001), a short description of the above results will also be given in this section.

Before describing the results obtained on the possible runout of the three Rosone landslide scenarios (§2.2), Forlati et al. 1991 gave an indication of the limitations of the adopted approach:
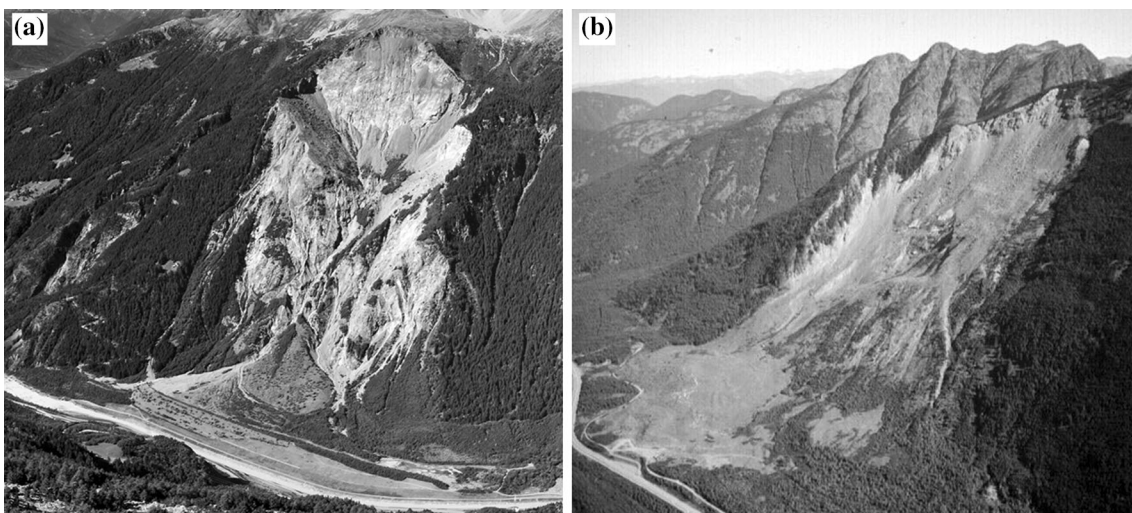
Fig. 7 a Val Pola rock avalanche (courtesy of Martin Mergili); **b** Hope rock avalanche (courtesy of Quaternary Geoscience Research Group)

Fig. 8 Runout paths.
a Elongated, **b** tongue, **c** T-shaped (modified after Nicoletti and Sorrivo-Valvo 1991)
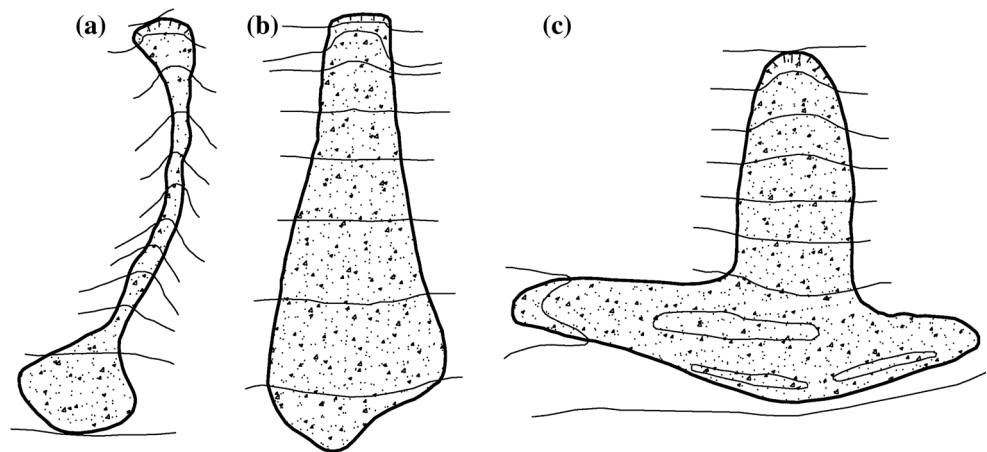
Table 2 RASH^{3D}-investigated range of rheological parameters

Frictional rheology	Voellmy rheology	
Friction angle, φ (°)	Friction coeff., μ (–)	Turbulence coeff., ξ (m/s^2)
16	0.1	200
18	0.1	500
20	0.2	500

1. A linear interpolation is used to describe the relation between the friction coefficient (tanα) and the mobilized volume. However, the data distribution is not normal for either the independent variable y (=log H/L) or the dependent variable x (=log V);
2. the number of considered past events is somewhat limited (33–76), and the type of landslides is inhomogeneous;
3. it is not clear whether the volume that has to be considered is the one that is measured at triggering or at deposition;
4. these methods neglect any confinement of the flowing mass;
5. these methods only provide an indication of the equivalent friction angle and a rough evaluation of the area potentially affected by the moving mass.

After these preliminary remarks, a swell factor of 30 % was assumed to account for the bulking processes during propagation and a 99.73 % confidence interval was considered by Forlati et al. 1991, who stated that using Scheidegger's (1973) and Li's (1983) empirical methods for the different scenarios, the mass could theoretically reach the area between the hamlets of Rosone (upper limit of the confidence interval) and Locana (lower limit of the confidence interval), which is about 4 km downstream

from Rosone. As discussed in detail in Sect. 5.1, none of the analyses carried out with RASH^{3D} shows that the mass deposit could reach Locana.

From a chronological point of view, the results obtained by Enel.Hydro (2001), with Friz and Pinelli's (1993) empirical method, should be now described. Since these results are the more exhaustive as far as the number of analyzed scenarios, spatial mapping and description of results are concerned, they will be the subject of a detailed comparison with RASH^{3D} results in Sect. 5.1.

For this reason, the DAN results are now commented on. Only one of the previously described scenarios (Scenario 1) was investigated using DAN and a Frictional rheology ($\varphi = 19.7°$) by Pirulli (2004). Since DAN is a pseudo-three-dimensional model, it requires that the lateral spreading of the mass along the runout path is given as input data. This spreading is not a result of the numerical analysis. As a consequence, the lateral spreading defined in the Enel.Hydro (2001) graphical interpretation of the topography was used.

For this reason, the DAN results have led to an improvement in the knowledge of the landslide velocity, the time at which the event finishes and the depth of the displaced mass in the deposition area for Scenario 1, but this knowledge is a function of the runout area defined by Enel.Hydro (Fig. 9).

However, a comparison between the DAN (Pirulli 2004) and RASH^{3D} results could be made, in terms of flow depth and velocity, for Scenario 1 and Frictional rheology.

DAN gives a maximum depth of the mass in the depositional area of about 32 m and a maximum velocity of the mass during propagation of about 48 m/s (Pirulli 2004). RASH^{3D} instead gives values of 27 m and 57 m/s considering a Frictional rheology and a friction angle equal to 20°. It is important to remember that unlike DAN, the shape of the runout path is not input data for RASH^{3D}.
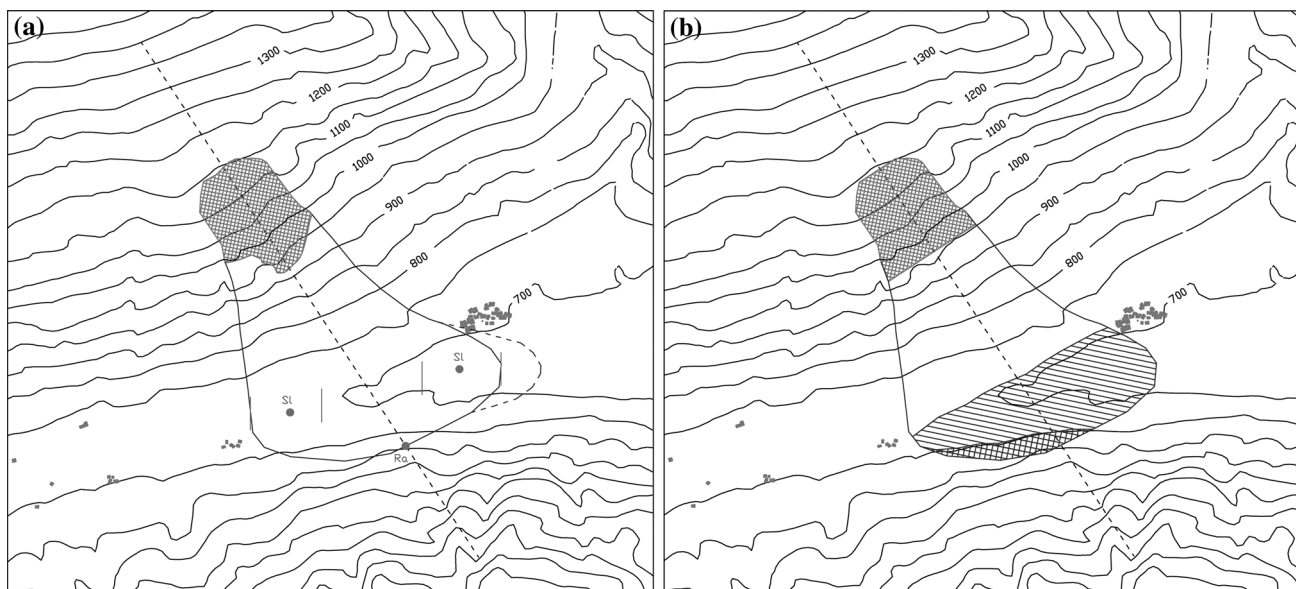
Fig. 9 Scenario 1. **a** Enel.Hydro results: the *solid line* indicates the runout area as being symmetric to the axial travel distance, the *dashed line* indicates the runout area in the case of a prevalent expansion in the direction of the valley; **b** DAN results for the Enel.Hydro symmetric runout area (modified after Amatruda et al 2004 and Pirulli 2004)

5.1 Comparison of the RASH[3D] and ENEL.HYDRO Results

As already mentioned, a dedicated section has been devoted to the comparison of the RASH[3D] and ENEL.-HYDRO results, since the latter represent the most comprehensive existing results pertaining to the possible evolution of the Rosone landslide.

A continuum mechanics-based model, such as RASH[3D], allows the different aspects that characterize the flow-dynamics of a rapid moving mass to be analyzed.

Starting from the main topic of interest of the authority responsible for territory management, attention is initially focused on the comparison between the shape of the runout area (i.e., propagation plus deposition) obtained by Enel.Hydro with an empirical approach and that obtained with RASH[3D].

A first comparison is carried out concerning Scenario 3, which is the most catastrophic one (Fig. 10). Superimposing the Enel.Hydro result onto each of the results obtained with RASH[3D] for both the Frictional and the Voellmy rheology in the investigated parameter range, it can be observed that the eastern part of the runout area defined by Enel.Hydro is in good agreement with many of the RASH[3D] results, and RASH[3D] almost always remains on the safe side (except in case of Fig. 10b). On the contrary, in the western side of the runout area, the Enel.Hydro result is always underestimated in comparison to the RASH[3D] results. RASH[3D] indicates that the Fornolosa hamlet could be struck by the landslide.

Moving on to Scenario 2 (Fig. 11), which is the intermediate one in terms of volume of mobilized material, it immediately emerges that the Enel.Hydro result is always underestimated in the eastern part of the mass runout in comparison to the RASH[3D] results. A certain similarity between the two approaches can be observed for this side of the deposit, but only when a Frictional rheology with a friction angle equal to 20° is adopted in RASH[3D] (Fig. 11f). The same observations as those of Scenario 3 can be made for the western side of the runout area, except for the fact that, in some of the RASH[3D] analyses, the Fornolosa hamlet appears totally or partially safe.

Finally, Scenario 1, which is the least catastrophic, but concerns the most active portion of the slope, is analyzed (Fig. 12). In this case, a certain fitting can be observed between the two approaches, but only when a Voellmy rheology, with a friction coefficient equal to 0.2 and a turbulence coefficient equal to 500 m/s², is adopted in RASH[3D] (Fig. 12c).

As far as the analysis of the mass deposit in the valley bottom is concerned, it emerges that this deposit could cause an obstruction of the Orco River with the consequent formation of a lake on the western side of the deposit. Once knowledge of the river discharge and the maximum depth of the deposit is available, it is possible to determine the basin extension and the time necessary to fill it completely. To determine the maximum depth of the deposit, Enel.Hydro assumed that the deposit had a wedge shape and an average slope of 18°. In this way, the maximum depth values given in Table 3 were obtained.
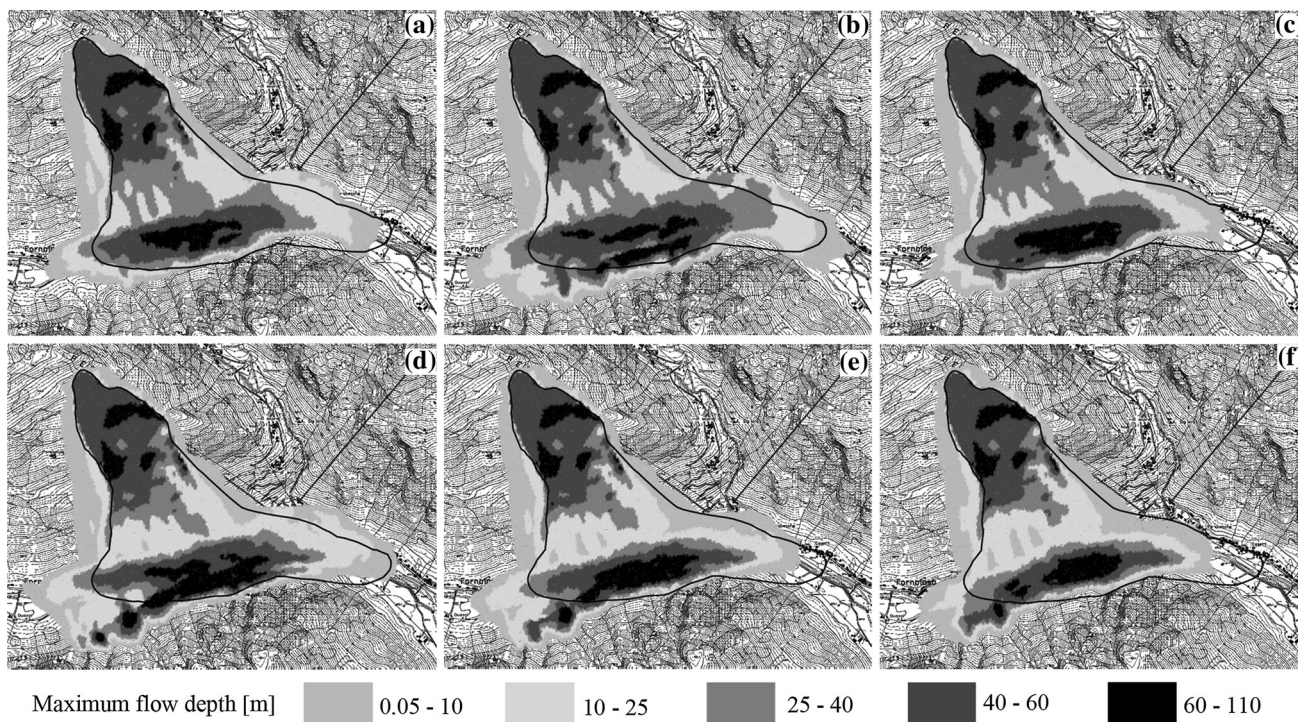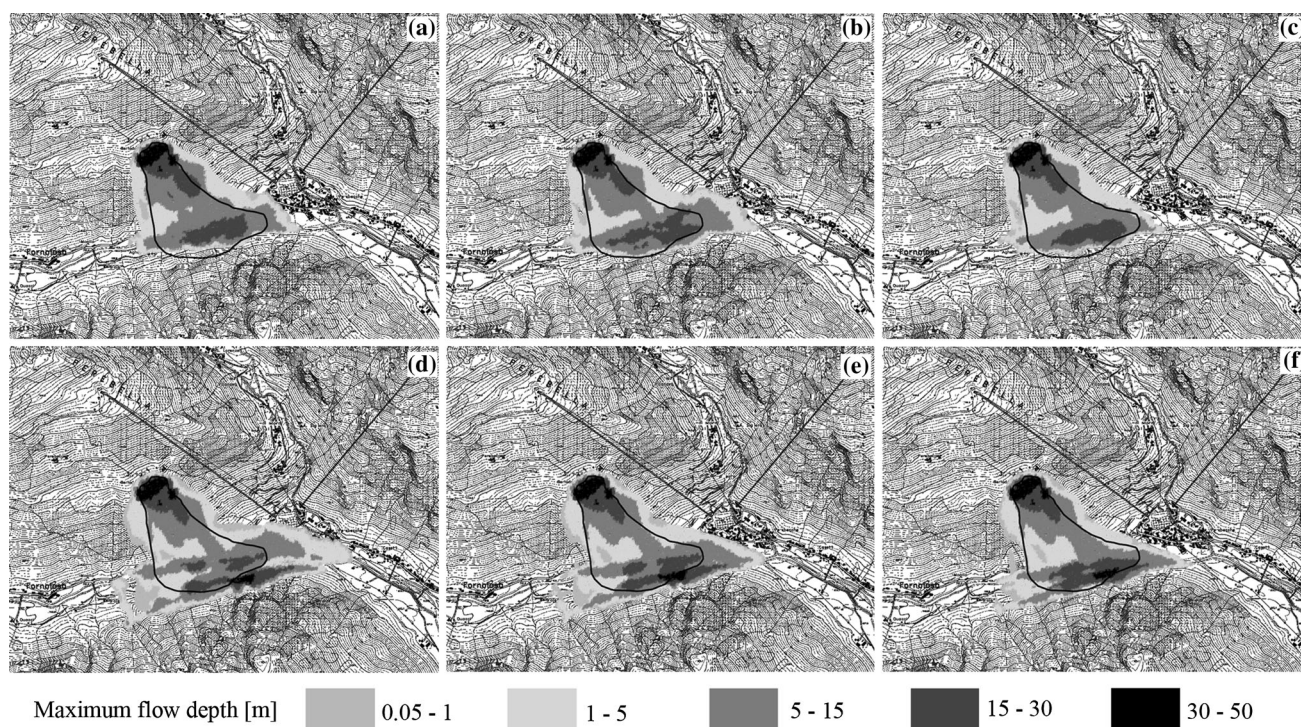
Fig. 10 Scenario 3. Comparison of the RASH[3D] (*shadowed area*) and Enel.Hydro (*solid line*) results in terms of computed runout area extension. RASH[3D] rheological parameters: Voellmy rheology: **a** $\mu = 0.1$, $\xi = 200$ m/s^2; **b** $\mu = 0.1$, $\xi = 500$ m/s^2; **c** $\mu = 0.2$, $\xi = 500$ m/s^2. Frictional rheology: **d** $\varphi = 16°$, **e** $\varphi = 18°$, **f** $\varphi = 20°$
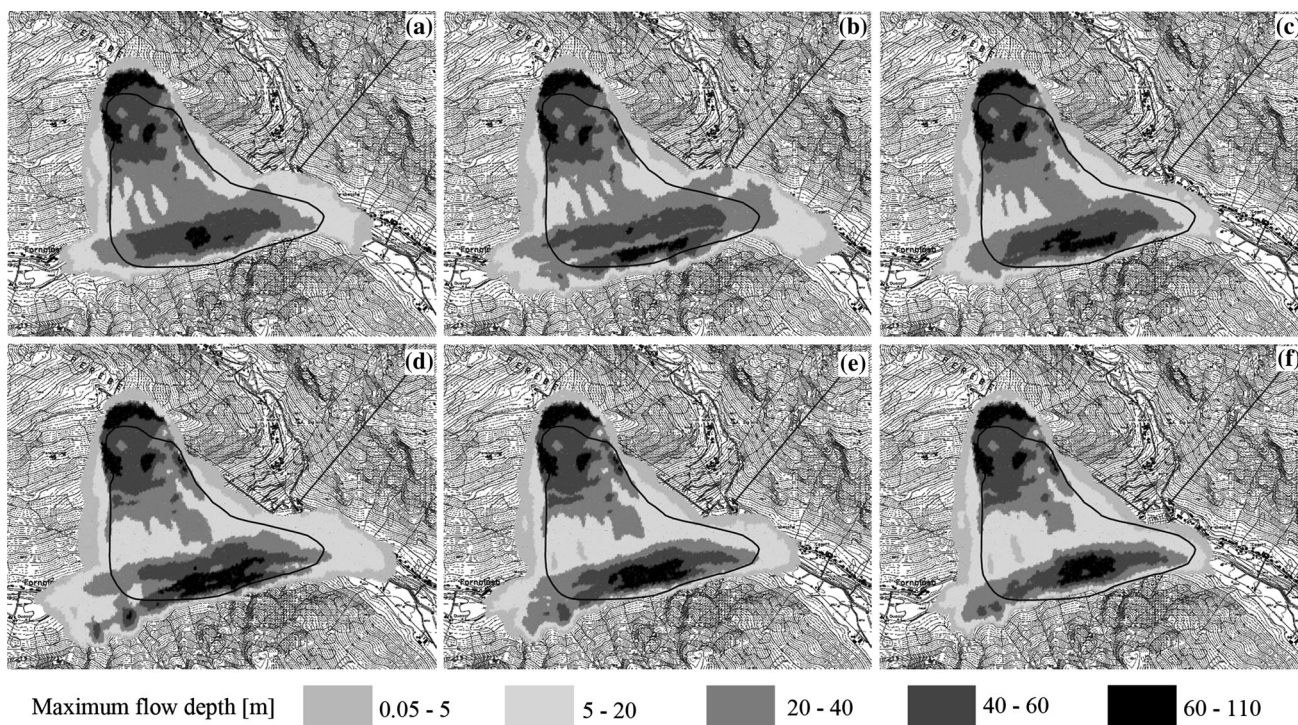
Fig. 11 Scenario 2. Comparison of the RASH[3D] (*shadowed area*) and Enel.Hydro (*solid line*) results in terms of computed runout area extension. RASH[3D] rheological parameters: Voellmy rheology: **a** $\mu = 0.1$, $\xi = 200$ m/s^2; **b** $\mu = 0.1$, $\xi = 500$ m/s^2; **c** $\mu = 0.2$, $\xi = 500$ m/s^2. Frictional rheology: **d** $\varphi = 16°$, **e** $\varphi = 18°$, **f** $\varphi = 20°$

Fig. 12 Scenario 1. Comparison of the RASH[3D] (*shadowed area*) and Enel.Hydro (*solid line*) results in terms of computed runout area extension. RASH[3D] rheological parameters: Voellmy rheology: **a** $\mu = 0.1$, $\xi = 200$ m/s[2]; **b** $\mu = 0.1$, $\xi = 500$ m/s[2]; **c** $\mu = 0.2$, $\xi = 500$ m/s[2]. Frictional rheology: **d** $\varphi = 16°$, **e** $\varphi = 18°$, **f** $\varphi = 20°$

Table 3 Enel.Hydro-maximum depth of the deposit

Scenario 1 (m)	Scenario 2 (m)	Scenario 3 (m)
35	65	95

On the other hand, RASH[3D] allows the depth of the mass to be known at each point of the final deposit as well as the maximum depth that the flowing mass has reached at each point of the valley bottom involved in the mass propagation. The spatial distribution can be observed for each scenario in Figs. 10, 11 and 12, while the maximum depth values on the valley bottom are summarized in Table 4 for the final deposit (H_{dep}) and during the event (H_{max}).

From a comparison of the two approaches it can be observed that the values estimated by Enel.Hydro are closer to H_{max} than to H_{dep}.

Further aspects that can be analyzed using the RASH[3D] code concern the velocity reached by the mass during propagation at each position and in each time step, and the maximum velocity distribution obtained throughout the entire process. This last piece of information is resumed for each rheology and each scenario in Table 5.

It can be observed that, for all of the analyzed scenarios, the Frictional rheology overestimates the velocity, compared to the Voellmy results. Similar behavior was

observed by Hungr and Evans (1996) when they back-analyzed 23 case histories of rock avalanches with three alternative rheologies: Frictional, Voellmy and Bingham. Having had the possibility of comparing calculated velocities with actual observations in terms of velocity, Hungr and Evans noticed that the Voellmy rheology gave an excellent correspondence of the calculated and observed velocities. The Frictional and Bingham models both overestimated the velocities. This trend had previously been noted for the frictional model by Körner (1976).

Furthermore, the velocity computed with RASH[3D] is comparable to other famous rock avalanches observed in other parts of the world. For example, the 1881 Elm rock avalanche in Switzerland (11×10^6 m[3]), which traveled at a maximum speed of 70 m/s (Hsu 1975), the 1903 Frank rock avalanche in Canada (3×10^6 m[3]), which traveled at a maximum speed of 40 m/s (Sosio et al. 2008), and the 1959 Madison Canyon rock avalanche in USA (30×10^6 m[3]) traveled at a maximum speed of 50 m/s (Hadley 1964). Therefore, the RASH[3D] results appear to be of the right order of magnitude.

Finally, a spatial distribution of the maximum velocities of the three investigated scenarios obtained with RASH[3D] is given as an example in Fig. 13, for a selected combination of Voellmy rheological parameters (i.e., 0.1–500 m/s[2]). It can be observed that the maximum velocity is

Table 4 RASH^{3D}-valley bottom: maximum depth during mass flowing of the mass (H_{max}) and after the final deposition of the mass (H_{dep})

Rheology	Scenario 1		Scenario 2		Scenario 3	
	H_{dep} (m)	H_{max} (m)	H_{dep} (m)	H_{max} (m)	H_{dep} (m)	H_{max} (m)
Voellmy						
0.1–200 m/s^2	20.69	25.92	51.96	72.16	60.19	80.44
0.1–500	18.18	28.71	43.61	83.15	51.06	96.04
0.2–500	24.66	26.23	56.81	84.06	63.51	92.12
Frictional						
16°	20.35	45.44	60.84	93.13	69.76	101.21
18°	23.22	42.74	62.39	89.74	70.55	94.62
20°	27.03	43.94	66.77	82.22	74.76	85.66

Table 5 RASH^{3D}-maximum velocity reached by the mass throughout the entire process

Rheology	Scenario 1 V_{max} (m/s)	Scenario 2 V_{max} (m/s)	Scenario 3 V_{max} (m/s)
Voellmy			
0.1–200 m/s^2	39.54	50.71	52.89
0.1–500	46.81	64.01	66.22
0.2–500	42.03	56.20	57.82
Frictional			
16°	66.27	79.54	87.64
18°	60.82	73.10	82.01
20°	57.33	65.56	76.44

reached by the mass in the lower part of the triggering slope.

6 Conclusions

This paper gives a brief description of the Rosone deep-seated gravitational slope deformation, with particular emphasis on the analysis of its potential evolution, in terms of a catastrophic rock avalanche.

Efforts have long been made to give an exhaustive description of the morphological and structural characteristics of this site. The result of these efforts is that the Bertodasco sector, which has been identified as the most active part of the DSGSD, can be divided into three main sectors with different rock mass evolutions and movements, here referred to as A, B and C. Three different possible evolution scenarios, with decreasing probability of occurrence and increasing impact on land planning, have been investigated in this work.

The modeling of the possible consequences of the catastrophic evolution of these scenarios has been the subject of analyses of different authors (Forlati et al. 1991; Enel.Hydro 2001; Pirulli 2004) and with different approaches. Among these, the most exhaustive analysis was made by Enel.Hydro, but none of the analyses used a three-dimensional continuum mechanics-based approach. Hence, the continuum mechanics-based RASH^{3D} code has been here used to run new analyses on the potential catastrophic evolution of the Rosone rock avalanche.

Two different rheological laws (Frictional and Voellmy) have been adopted and a range of rheological values has been investigated for each rheology. The range of each rheological value has been obtained from the literature by selecting the rheological values that were computed through the back-analysis of past events with similar characteristics to the here investigated case.

An analysis of the obtained results has pointed out that the first advantage of using the RASH^{3D} code is that it offers the possibility of simulating the propagation of the mass using a real three-dimensional topography (i.e., the Digital Elevation Model). In fact, simplified codes that can only analyze single topographical sections can neither investigate the lateral spreading of the mass nor simulate a change in the flowing direction of the movement (e.g., the presence of a narrow valley transversal to the main direction of the flow propagation can cause a run-up of the mass on the opposite slope and a change in the flowing direction).

The possibility of studying the flowing mass in three dimensions allows the shape of the runout area to be defined not only from point information. In RASH^{3D}, the runout area is an output of the code, and both spatial and temporal information of the flow depth and velocity are made available.

A comparison of the Forlati et al. (1991) and RASH^{3D} results has shown that none of the analyses carried out with RASH^{3D} determines a direct deposition of the mass in Locana, as was instead observed with the empirical methodology applied by Forlati et al.

A comparison of the Enel.Hydro (2001) and RASH^{3D} results has evidenced that:

– the former underestimates the extension of the runout area when compared to the latter;

Maximum flow velocity [m/s]

0 - 8	20 - 35	50 - 70
8 - 20	35 - 50	
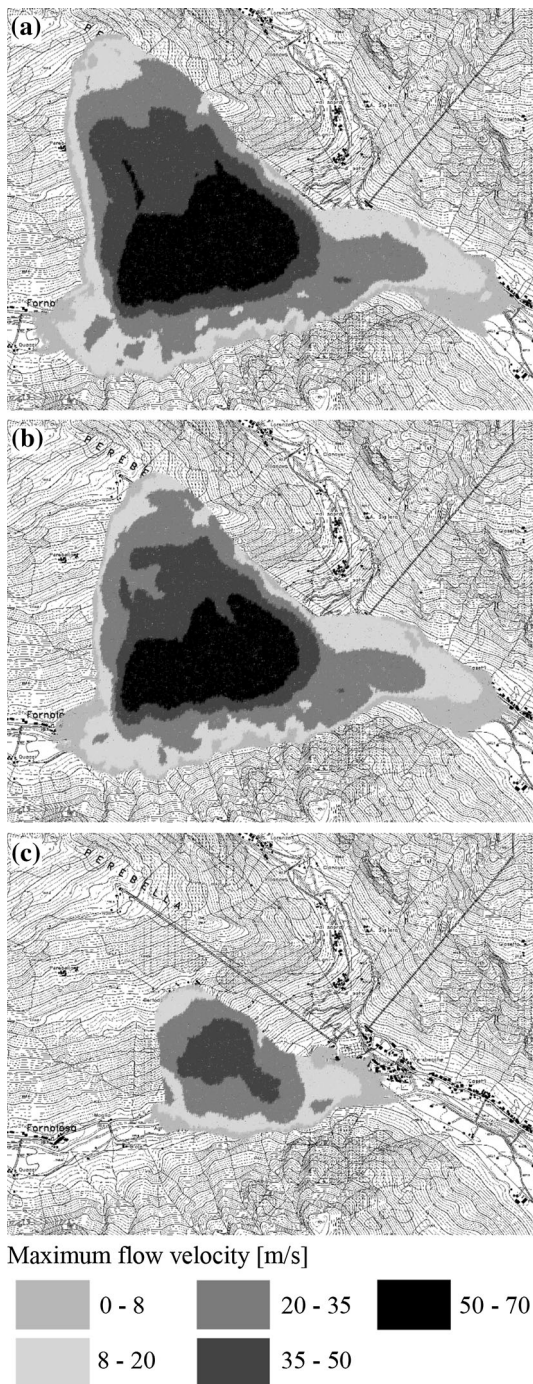
Fig. 13 Spatial distribution of the maximum velocity computed with RASH[3D] using a Voellmy rheology with $\mu = 0.1$ and $\xi = 500$ m/s[2]. **a** Scenario 3; **b** Scenario 2; **c** Scenario 1

– the former overestimates the maximum depth of the deposit in the valley bottom compared to the latter.

A comparison could be made between the DAN (Pirulli 2004) and RASH[3D] results in terms of flow depth and velocity, but not in terms of runout area, since the runout area used in DAN is the graphical interpretation of the

topography made by Enel.Hydro in 2001. As far as the maximum flow depth at deposition and velocity during propagation are concerned, it has been observed that RASH[3D] slightly underestimates the depth and overestimates the velocity for Scenario 1 compared to DAN. As already mentioned, the same trend is observed when the RASH[3D] and Enel.Hydro results are compared in terms of maximum flow depth at deposition.

In conclusion, the use of a continuum mechanics-based code, such as RASH[3D], can result in a great deal of information on the dynamics of the propagation of rock avalanche events; in particular, compared to previous analyses, the shape of the runout path is not an input of the code, but is a result of the analysis. The spatial distribution of the velocity and depth during the runout and after deposition of the material can be computed as well as the consequences of a possible runup of the flowing mass on the opposite slope. However, the main problem is still that of calibrating the rheological parameters. In fact, the use of a selected set of values calibrated through the back-analysis of past events has been proposed here.

As for the consequences on the area that could be impacted by the Rosone landslide, all the analyses conducted with the different methodologies have evidenced the problem of a possible obstruction of the Orco River on the valley bottom and the possible formation of a lake.

The presence of a lake would endanger downstream areas in the case of overflows, or even worse, in the case of dam breaks. A wave could also originate if more material were to be released from the slope, in the form of a landslide, and to fall into the above-mentioned lake (e.g., the Vajont effect).

Such a lake could form over a short or long period of time, as a function of the maximum depth and shape of the landslide deposit in the valley bottom, and could contain different quantities of water. However, the Ceresole dam (15 km upstream from the Rosone area) could retain water and give the Civil Protection the time necessary to arrange targeted interventions, unless the Rosone landslide were to collapse because of overloading of the hydrographic network and then the Ceresole dam were to already be filled. In fact, owing to dam filling, huge quantities of water had already been released from the Ceresole dam in the past during heavy rainfalls (e.g., 1947, 1977). In similar conditions, the consequences on the area surrounding the landslide deposit are easy to imagine, in terms of both filling of the landslide dam lake and safety of the population (Forlati et al. 1991).

Besides the problems connected to the creation of a landslide dam lake, dam overflows and dam breaks, the underestimation of the extension of the valley bottom area that could be directly impacted by the landslide could produce serious consequences for some hamlets located at

the borders of the runout area. The RASH^{3D} analysis results have in particular pointed out the possibility of the Fornolosa hamlet being affected by a landslide. However, taking into account (1) that the analyzed scenarios only refer to a part of a wider DSGSD and that other sectors of the slope could also destabilize, (2) that instead of an all at once release of the material, a progressive failure could occur and (3) that no considerations have been made on the possible wind and dust effects, it should be noted that in the case of an emergency, the results of the hypothesized scenarios should be combined with an attentive and actual evaluation of the current conditions.

References

Amatruda G, Campus S, Castelli M, Delle Piane L, Forlati F, Morelli M, Paro L, Piana F, Pirulli M, Polino R, Ramasco M, Scavia C (2004) The Rosone landslide (chapter 5). In: Bonnard CH, Forlati F, Scavia C (eds) "Identification and mitigation of large landslide risks in Europe. Advances in risk assessment". A.A. Balkema publishers, pp 89–136

Audusse E, Bristeau MO, Perthame BT (2000) Kinetic schemes for Saint-Venant equations with source terms on unstructured grids. Institut National de Recherche en Informatique et en Automatique, Report 3989, LeChesnay, France

Bristeau MO, Coussin B (2001) Boundary conditions for the shallow water equations solved by kinetic schemes. Institut National de Recherche en Informatique et en Automatique, Report 4282, LeChesnay, France

Compagnoni R, Elter G, Lombardo B (1974) Eterogeneità stratigrafica del complesso degli gneiss minuti nel massicci cristallino del Gran Paradiso. Mem Soc Geol It. 13(1):227–239

Delle Piane L, Fontan D, Mancari G (2010) The Rosone landslide (Orco River valley, Western Italian Alps); un updated model. Geogr Fis Dinam Quat 33:165–177

Dutto F, Friz E (1989) Ricerche sul comportamento di grandi france nelle alpi, Rapporto interno CNR-IRPI/ISMES Febbraio, p 16

Enel.Hydro (2001) Attività di progettazione, fornitura ed installazione di un sistema di monitoraggio integrato del movimento franoso di Rosone - Scenari di rischio - Valutazione dell'area di invasione conseguente all'ipotetico collasso della frana come valanga di roccia e definizione dei livelli di soglia e delle procedure di allertamento. Internal Report Prog. ISMES 2338, Doc. RAT-ISMES-1432/2001

Fell R, Glastonbury J, Hunter G (2007) Rapid landslides: the importance of understanding mechanisms and rupture surface mechanics. Quat J Eng Geol Hydrogeol 40:9–27

Forlati F, Ramasco M, Susella G, Barla G, Marino M, Mortara G (1991) La deformazione gravitativa di Rosone. Un approccio conoscitivo per la definizione di una metodologia di studio, In: Proc. Conference on "Fenomeni franosi. Interventi di salvaguardia del territorio e proposte per la pianificazione urbanistica", Studi Trentini di Scienze Naturali, Acta Geologica 68:71–108 **(in Italian)**

Forlati F, Gioda G, Scavia C (2001) Finite element analysis of a deep-seated slope deformation. Rock Mech Rock Eng 34:135–159

Friz E, Pinelli PF (1993) Ricerche sull'area di invasione di valanghe di roccia. Proc. National Congress "Fenomeni Franosi", Riva del Garda, Italy. Studi Trentini di Scienze Naturali, Acta Geologica 68:55–65 **(in Italian)**

Hadley JB (1964) Landslides and related phenomena accompanying the Hebgen Lake earthquake of August 17, 1959. U.S. Geol Surv Prof Paper 435:107–138

Heim A (1932) Bergsturz und Menschenleben. Fretz and Wasmuth Verlag A.G, Zürich

Hsu KJ (1975) Catastrophic debris streams (sturzstroms) generated by rockfalls. Bull Geol Soc Am 86:129–140

Hungr O (1995) A model for the runout analysis of rapid flow slides, debris flows, and avalanches. Can Geotech J 32:610–623

Hungr O, Evans SG (1996) Rock avalanche runout prediction using a dynamic model. In: Senneset K (ed) Proceedings of the 7th International Symposium on Landslides, Trondheim. A.A. Balkema, Rotterdam, pp 233–238

Hungr O, Evans SG, Bovis M, Hutchinson JN (2001) Review of the classification of landslides of the flow type. Environ Eng Geosci 7:221–238

Hungr O (2002) Rock avalanche motion: process and modelling, In NATO advanced research workshop massive rock slope failure: new model of hazard assessment, June 16-21, Celano, Italy

Hungr O, Evans SG (2004) Entrainment of debris in rock avalanches: an analysis of a long runout mechanism. Geol Soc Am Bull 116(9/10):1240–1252

Hungr O (2006) Rock avalanche occurrence, process and modelling. In: Evans SG et al (eds) Landslides from massive rock slope failure, NATO Science Series, Springer 49:243–266

Hutchinson JN (1986) A sliding-consolidation model for flow slides. Can Geotech J 23:115–126

Iverson RM, Denlinger RP (2001) Flow of variably fluidized granular masses across three dimensional terrain—1: coulomb mixture theory. J Geophys Res 106(B1):537–552

Kilburn C, Sorensen SA (1998) Runout lengths of sturzstroms: the control of initial conditions and of fragment dynamics. J Geophys Res 103:17877–17884

Körner HJ (1976) Reichweite un Geschwindigkeit von Berstruzen und fleisscheneelawinen. Rock Mech 8(4):225–256 **(in German)**

Li T (1983) A mathematical model for predicting the extent of a major rockfall. Zeitsch Geomorph 27:473–482

Luino F, Ramasco M, Susella G (1993) Atlante dei centri abitati instabili piemontesi (classificati ai sensi della L. 9 Luglio 1908 n. 445 e seguenti). CNR I.R.P.I./Regione Piemonte S.P.R.G.M.S., Gruppo Nazionale per la Difesa dalle Catastrofi Ecologiche. 964: Programma Speciale Studio Centri Abitati Instabili

McDougall S, Pirulli M, Hungr O, Scavia C (2008) Advances in landslide continuum dynamic modeling (Special Lecture). In: 10th international symposium on landslides and engineered slopes, Xi' An, China, 30 June-4 July, pp 835–841

Nicoletti G, Sorriso-Valvo M (1991) Geomorphic control of the shape and mobility of rock avalanches. Geol Soc Am Bull 103:1365–1373

Notti D, Meisina C, Colombo A, Lanteri L, Zucca F (2013a) Studying and monitoring large landslides with persistent scattered data. Ital J Eng Geol Environ Book Series 6:349–360

Notti D, Meisina C, Zucca F, Balduzzi G, Colombo A (2013b) Map numerical modelling of landslides using data from different monitoring systems: the example of Rosone (Western Alps). In: Procs. IAEG XII Congress, Torino September 15–19, 2014, 2:1455–1459

Perla R, Cheng TT, McClung DM (1980) A two-parameter model of snow-avalanche motion. J Glaciol 26(94):197–207

Pirulli M (2004) Numerical analysis of three potential rock avalanches in the Alps. Felsbau 22(2):32–38

Pirulli M (2005) Numerical modelling of landslide runout, a continuum mechanics approach. PhD Thesis, Politecnico di Torino, Torino, Italy

Pirulli M, Mangeney A (2008) Results of back-analysis of the propagation of rock avalanches as a function of the assumed rheology. Rock Mech Rock Eng 41(1):59–84

Pirulli M, Marco F (2010) Description and numerical modelling of the October 2000 Nora debris flow, Northwestern Italian Alps. Can Geotech J 47:135–146

Pisani G, Castelli M, Scavia C (2010) Hydrogeological model and hydraulic behaviour of a large landslide in the Italian Western Alps. Nat Hazards Earth Syst Sci 10:2391–2406

Ramasco M, Stoppa T, Susella G (1989) La deformazione gravitativa profonda di Rosone nella Valle dell'Orco. Bollettino della Società Geologica Italiana 108:401–408

Ramasco M, Troisi C (2003) Grandi fenomeni franosi attivatisi a seguito dell'evento dell'ottobre 2000. Eventi alluvionali in Piemonte—evento alluvionale regionale del 13-16 ottobre 2000. ARPA Piemonte, Torino, pp 255–309

Revellino P, Hungr O, Guadagno FM, Evans SG (2004) Velocity and runout simulation of destructive debris flows and debris avalanches in pyroclastic deposits, Campania region, Italy. Environ Geol 45:295–311

Rickenmann D, Koch T (1997) Comparison of debris flow modelling approaches, In: Chen CL (ed) Proc. 1st Int. Conf. On Debris Flow Hazards Mitigation: Mechanics, Prediction, and Assessment ASCE, Reston, Va., 576–585

Savage SB, Hutter K (1989) The motion of a finite mass of granular material down a rough incline. J Fluid Mech 199:177–215

Scheidegger A (1973) On the prediction of the reach and velocity of catastrophic landslides. Rock Mech 5:231–236

Sosio R, Crosta GB, Hungr O (2008) Complete dynamic modeling calibration for the Thurwieser rock avalanche (Italian Central Alps). Eng Geol 100(1–2):11–26

Varnes DJ (1978) Slope movement types and processes. In Schuster RJ and Krizek RJ (eds), Landslides, analysis and control: transportation research board, National academy of sciences, Washington, DC., Special Report 176:11–33

Voellmy A (1955) Uber die Zerstorungskraft von Lawinen. Schweizerische Bauzeitung 73:212–285 **(in German)**